

# NUMERICALLY INVARIANT SIGNATURE CURVES

MIREILLE BOUTIN

ABSTRACT. Corrected versions of the numerically invariant expressions for the affine and Euclidean signature of a planar curve introduced by Calabi et al. in [COS<sup>+</sup>98] are presented. The new formulas are valid for fine but otherwise arbitrary partitions of the curve. We also give numerically invariant expressions for the four differential invariants parameterizing the three dimensional version of the Euclidean signature curve, namely the curvature, the torsion and their derivatives with respect to arc length.

## 1. INTRODUCTION

The concept of signature was introduced by Calabi et al. [COS<sup>+</sup>98] as “a new paradigm for the invariant recognition of visual objects.” For the case of planar curves, the signature is defined as follows: if  $\alpha(s)$  is an analytic curve in  $\mathbb{R}^2$  parameterized by  $G$ -arc length  $s$  and if  $G$  is any finite dimensional transformation group acting transitively on  $\mathbb{R}^2$ , then the signature curve  $S$  of  $\alpha(s)$  with respect to  $G$  is given parametrically as  $(\kappa(s), \kappa_s(s))$ , where  $\kappa$  is the  $G$ -invariant curvature and  $\kappa_s$  its derivative with respect to arc length. One of the consequences of a theorem proved by Cartan [Car35] is that  $S$  fully determines the given curve  $\alpha$  modulo  $G$ .

The signature curve can therefore be used to program a computer for recognizing curves modulo certain group transformations. However differential invariants involve high order derivatives and hence are very sensitive to round off errors and noise. The idea of writing a numerical scheme in terms of joint invariants was also introduced by Calabi et al. [COS<sup>+</sup>98]. Hoping to obtain less sensitive approximations, they suggested finding numerical expressions for  $\kappa$  and  $\kappa_s$  in terms of joint invariants. A joint invariant of the action of a group on a manifold is a real valued function  $J$  which depends on a finite number of points  $x_1, \dots, x_n$  of the manifold and which remains unchanged under the simultaneous action of the group  $G$  on the point configuration, i.e.  $J(x_1, \dots, x_n) = J(g \cdot x_1, \dots, g \cdot x_n), \forall g \in G$ . For example,

the Euclidean distance between two points is a joint invariant of the action of the Euclidean group on  $\mathbb{R}^2$ . Expressing differential invariants in terms of joints invariants results in a  $G$ -invariant numerical approximation. In their paper, Calabi et al. proposed numerically invariant expressions for  $\kappa$  and  $\kappa_s$  for two specific group actions, namely the proper Euclidean group and the equi-affine group.

But contrary to their claim, the expressions given for  $\kappa_s$  are not convergent for arbitrary partitions of the curve. In the next section, we give correct formulas for approximating  $\kappa_s$  and explain why the old ones do not work in general. In order to prove our claims, we also compute the resulting numerical signatures in a practical example with a variety of different partitions. We then compare with the signatures obtained with the old formulas. We also test and compare both formulas on noisy data.

Cartan's theorem also provides us with a way to characterize curves in  $\mathbb{R}^3$  modulo a group transformation. The generalization of the signature curve is a curve in  $\mathbb{R}^4$  determined by four differential invariants: the  $G$ -invariant curvature  $\kappa$ , its derivative  $\kappa_s$  with respect to  $G$ -invariant arc length  $s$ , the  $G$ -invariant torsion  $\tau$  and its derivative  $\tau_s$  with respect to  $s$ . For practical applications, we are interested in the case where  $G$  is the proper Euclidean group. Following the example of [COS<sup>+</sup>98], we have found approximations for  $\kappa$ ,  $\kappa_s$ ,  $\tau$  and  $\tau_s$  in terms of the simplest joint invariant of the action of the Euclidean group on  $\mathbb{R}^3$ : the Euclidean distance. The results are given in section 3. That section also contains the results of numerical tests performed on a space curve with different parameterizations.

## 2. CORRECTIONS FOR THE CASE OF A PLANAR CURVE

In principle, one must keep track of the order of the approximation when manipulating an approximation. This is especially true when trying to approximate a derivative using an approximate expression. For example, if  $\tilde{c}(t) = c(t) + O(t)$  is a first order approximation for  $c(t)$ , then for  $0 < t \ll 1$

$$\frac{\tilde{c}(t) - \tilde{c}(0)}{t} = \frac{c(t) + O(t) - c(0)}{t} = c'(0) + O(t^0)$$

is in general *not* an approximation for  $c'(0)$ .

Throughout this paper, we shall write

$$f(x_1, \dots, x_k) = g(x_1, \dots, x_k) + O(n),$$

whenever

$$f(x_1, \dots, x_k) = g(x_1, \dots, x_k) + \sum_{\substack{i_1, \dots, i_k=0 \\ i_1 + \dots + i_k \geq n}}^{\infty} c_{i_1 \dots i_k} x_1^{i_1} \dots x_k^{i_k},$$

and be careful not to drop the  $O(n)$  term until the end of our computations.

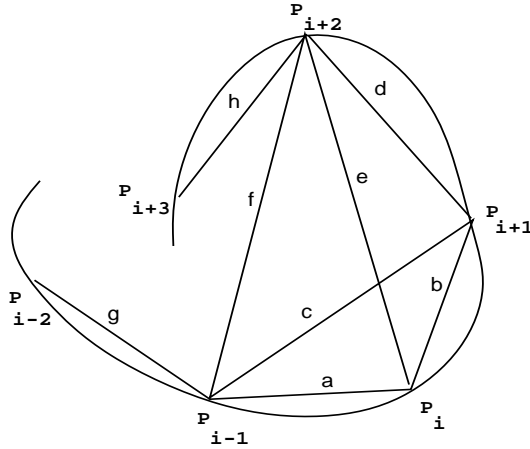
By keeping track of the order of approximation throughout the computations performed in [COS<sup>+</sup>98], one finds out that the expressions given for  $\kappa_s$  will converge only for a  $2^{nd}$  order approximation of  $\kappa$ . In the case of a regular partition of the curve, the approximations used for the curvature are of second order, as one can see from equation (1) below. This fortunate fact explains the correct numerical results presented in [COS<sup>+</sup>98]. However, for a generic partition there is no guarantee of success and failure is likely as we show by example.

In the following we present the corrected formulas together with their justification for the Euclidean and affine group action.

**2.1. Euclidean Group Action.** Let  $P_{i-2}$ ,  $P_{i-1}$ ,  $P_i$ ,  $P_{i+1}$ , and  $P_{i+2}$  be 5 consecutive points on a smooth planar curve. Denote by  $d(P_j, P_k)$  the Euclidean distance between the points  $P_j$  and  $P_k$ . As illustrated in Figure 1, let

$$\begin{aligned} a &:= d(P_{i-1}, P_i), & c &:= d(P_{i-1}, P_{i+1}), & e &:= d(P_i, P_{i+2}), & g &:= d(P_{i-2}, P_{i-1}) \\ b &:= d(P_i, P_{i+1}), & d &:= d(P_{i+1}, P_{i+2}) & f &:= d(P_{i-1}, P_{i+2}) \end{aligned}$$

FIGURE 1. Definition of Variables Used for Distances



It was shown in [COS<sup>+</sup>98] that  $\tilde{\kappa}(P_i) = \pm \frac{4\Delta}{abc}$ , where  $\Delta$  denotes the area of the triangle with sides of length  $a$ ,  $b$  and  $c$ , is a good approximation for the Euclidean

curvature at  $P_i$ . In fact, the following expansion has been proven to be valid for small  $a$  and  $b$ .

$$(1) \quad \tilde{\kappa}(P_i) = \kappa(P_i) + \frac{1}{3}(b-a)\kappa_s(P_i) + O(2).$$

Observe that  $\tilde{\kappa}$  depends only on the distances between the three points. Since the distance is a Euclidean invariant, we thus have a Euclidean numerically invariant expression for the curvature.

When  $a \neq b$ , the approximation obtained is only of first order. Therefore care must be taken when approximating the derivative  $\kappa_s(P_i)$ . The formulas used in [COS<sup>+</sup>98] are

$$(2) \quad \tilde{\kappa}_{s,1}(P_i) := \frac{\tilde{\kappa}(P_{i+1}) - \tilde{\kappa}(P_i)}{b},$$

$$(3) \quad \tilde{\kappa}_{s,2}(P_i) := \frac{\tilde{\kappa}(P_{i+1}) - \tilde{\kappa}(P_{i-1})}{c}.$$

We would like to have expressions that do not assume a priori conditions on the parameterizations. Hence we propose the following numerically Euclidean invariant expression for  $\kappa_s(B)$ :

$$(4) \quad \tilde{\kappa}_{s,3}(P_i) := 3 \cdot \frac{\tilde{\kappa}(P_{i+1}) - \tilde{\kappa}(P_i)}{a+b+d},$$

$$(5) \quad \tilde{\kappa}_{s,4}(P_i) := \frac{3}{2} \cdot \frac{\tilde{\kappa}(P_{i+1}) - \tilde{\kappa}(P_i)}{a+b+d} + \frac{3}{2} \cdot \frac{\tilde{\kappa}(P_i) - \tilde{\kappa}(P_{i-1})}{a+b+g},$$

$$(6) \quad \tilde{\kappa}_{s,5}(P_i) := 3 \cdot \frac{\tilde{\kappa}(P_{i+1}) - \tilde{\kappa}(P_{i-1})}{2a+2b+d+g}.$$

**Claim 2.1.** *Formulas (4), (5) and (6) converge to  $\kappa_s(P_i)$  as  $a, b, d, g \rightarrow 0$*

*Proof.* By (1) we have

$$\tilde{\kappa}(P_i) = \kappa(P_i) + \frac{1}{3}(b-a)\kappa_s(P_i) + O(2)$$

and

$$\tilde{\kappa}(P_{i+1}) = \kappa(P_{i+1}) + \frac{1}{3}(d-b)\kappa_s(P_{i+1}) + O(2).$$

Assume that  $\alpha = \alpha(s)$  is a smooth curve parameterized by arc length, that  $P_i = \alpha(0)$  and that  $P_{i+1} = \alpha(h)$ . We can write

$$\kappa(P_{i+1}) = \kappa(P_i) + h\kappa_s(P_i) + O(2) = \kappa(P_i) + b\kappa_s(P_i) + O(2)$$

and

$$\kappa_s(P_{i+1}) = \kappa_s(P_i) + O(1).$$

Thus

$$\tilde{\kappa}(P_{i+1}) - \tilde{\kappa}(P_i) = \frac{1}{3}(d - 2b + a)\kappa_s(P_i) + b\kappa_s(P_i) + O(2).$$

Rearranging, we obtain

$$3 \cdot \frac{\tilde{\kappa}(P_{i+1}) - \tilde{\kappa}(P_i)}{a + b + d} = \kappa_s(P_i) + O(1)$$

Therefore (4) is valid.

Expression (5) is just a symmetric formula obtained by averaging (4) with its reflected version. We obtain (6) by expanding  $\tilde{\kappa}(P_{i+1}) - \tilde{\kappa}(P_{i-1})$  about  $P_i$  in a similar way.  $\square$

Figures 2-8 show some experimental results obtained with non-noisy data. We constructed three different parameterizations of the exact curve  $r = 1 + \frac{1}{10} \cos t$ , for  $0 \leq t \leq 2\pi$ . The first one is the very regular partition obtained by setting  $t_1 = 0$  and  $t_{i+1} = t_i + \Delta t$  with  $\Delta t = 0.05$ ,  $i = 1, \dots, 125$ , for a total of 126 points. The second one is the irregular partition obtained by setting  $t_1 = 0$ ,  $t_{i+1} = t_i + 0.1\Delta t$  and  $t_{i+2} = t_i + 2\Delta t$  with  $\Delta t = 0.05$ , for  $i = 1, 3, 5, \dots$ , up to a total of 126 points. The last one is the very irregular partition obtained by setting  $t_1 = 0$ ,  $t_{i+1} = t_i + 0.2\Delta t$ ,  $t_{i+2} = t_i + 0.3\Delta t$ ,  $t_{i+3} = t_i + 3 * \Delta t$  with  $\Delta t = 0.05$ , for  $i = 1, 4, 7, \dots$ , up to a total of 126 points. For simplicity and in order to avoid confusion related to the time step, the corresponding signatures are only plotted for the values corresponding to  $i = 2, 3, \dots, 124$ .

The results illustrated in these figures show that our formulas are just as good as (2) and (3) when the parameterization is very regular. But when the parameterization is not, we see that (2) and (3) diverge from the exact solution, while (4), (5) and (6) remain closer to it. Thus we believe that our formulas are better for a generic partition of the curve. Observe that formula (4) suffers from a small bias due to its asymmetry. This phenomenon was also observed for formula (2) in [COS+98].

Figures 9-10 show some experimental results with data obtained from an actual image. We took the picture of a washer and segmented it to obtain the outside boundary of the washer. The curve obtained was very noisy so we first had

to smooth it. We did so via a fast Fourier transform algorithm. The smoothed boundary is shown in Figure 9.

Since the signature of a circle is ( $\kappa = \text{constant}, \kappa_s = 0$ ), we were hoping the signature of the approximated boundary would be close to being a point on the  $x$ -axis. We compared the results obtained with (3) and (6) for the 200 data points emphasized in bold on the graph of the segmented boundary. As shown by the graph of the corresponding signatures, both signatures are close to a point, although the results obtained with (6) are better.

**2.2. Affine Group Action.** Let  $\alpha$  be a convex smooth curve. Let  $P_0, P_1, P_2, P_3, P_4$  be five consecutive points on  $\alpha$ . Denote by  $[ijkl]$  the signed area of the parallelogram whose sides are  $P_i - P_j$  and  $P_k - P_l$  and by  $[ijk]$  the signed area of the parallelogram whose sides are  $P_i - P_j$  and  $P_i - P_k$ . Define  $T$  and  $S$  at  $P_2$  by

$$4 \cdot T(P_2) = \prod_{0 \leq l < m < n \leq 4} [lmn],$$

$$4 \cdot S(P_2) = [013]^2[024]^2[1234]^2 + [012]^2[034]^2[1324]^2$$

$$- 2[012][034][013][024]([123][234] + [124][134]).$$

Observe that the expressions for  $T$  and  $S$  are equi-affine invariant. The following is a numerically invariant approximation for the affine curvature at  $P_i$ :

$$(7) \quad \bar{\kappa}(P_i) = \frac{S(P_i)}{T(P_i)^{2/3}}.$$

Indeed the following expansion has been shown to be valid for sufficiently close points [COS<sup>+</sup>98]

$$(8) \quad \bar{\kappa}_i = \kappa + \frac{1}{5} \left( \sum_{j=i-2}^{i+2} L_j \right) \frac{d\kappa}{ds} + \dots$$

where  $L_j$  denotes the signed affine arc length of the conic from  $P_i$  to  $P_j$  and the higher order terms are quadratic in the  $L_j$ 's. Again, since this is a first order approximation, care must be taken when approximating the derivative of  $\kappa$  with respect to affine arc length  $s$ .

The formula used in [COS<sup>+</sup>98] is

$$(9) \quad \bar{\kappa}_{s,1} = \frac{\bar{\kappa}(P_{i+1}) - \bar{\kappa}(P_{i-1})}{\bar{S}_i + \bar{S}_{i-1}},$$

where  $\bar{S}_j$  is the triangular approximation to the affine arc length from  $P_j$  to  $P_{j+1}$ . This formula would be valid only if  $\bar{\kappa}$  were a second order approximation of  $\kappa$ . However, this is not the case unless  $\sum_{j=i-2}^{i+2} L_j$  is small compared to all of the  $L_j$ 's. We would like a more general expression. Hence we propose the following numerically affine invariant expression for  $\kappa_s$  which does not assume a priori conditions on the parameterizations:

$$(10) \quad \bar{\kappa}_{s,2}^1 = 5 \cdot \frac{\bar{\kappa}(P_{i+1}) - \bar{\kappa}(P_{i-1})}{\bar{S}_{i-3} + 2\bar{S}_{i-2} + 2\bar{S}_{i-1} + 2\bar{S}_i + 2\bar{S}_{i+1} + \bar{S}_{i-2}}$$

The convergence can be proved by an argument similar to the one used in the Euclidean case.

Figures 11-14 show the results obtained with our formula using different partitions of a curve. Comparison is made with the signature curve obtained with (9). As in the Euclidean case, we see that equations (9) and (10) seem just as good when the partition of the curve is regular. But when the partition is not regular, (9) diverges from the exact solution while (10) remains valid.

Figures 15-16 compare the result obtained with (9) and (10) using data obtained from an actual picture. We took the picture of the washer shown in Figure 9 and tried to compute the affine signature of the outside circle using (9) and (10). In both cases, we had to smooth the boundary quite a bit before we obtained sensible results. Again we did so using a fast Fourier transform algorithm. The smoothed boundary used is shown in Figure 15. We graphed the results corresponding to the piece of the smoothed boundary emphasized in bold. We see no significant difference between the signature obtained with (9) and (10). In fact, with all of the noisy data we tried, we obtained either diverging results or almost identical results for both formulas. This is most likely because the parameterizations we used gave us a second order approximation of the affine curvature  $\kappa$ .

### 3. NUMERICALLY INVARIANT EUCLIDEAN SIGNATURE FOR A SPACE CURVE

The signature curve  $S$  of a space curve is given by  $S = (\kappa, \kappa_s, \tau, \tau_s)$ . In the following section, we present some numerically Euclidean invariant approximations for  $S$  for the case of the Euclidean group action on  $\mathbb{R}^3$ . This is achieved by expressing each of the differential invariants constituting  $S$  in terms of Euclidean distances, which is the simplest joint invariant of the Euclidean group action on  $\mathbb{R}^3$ .

**3.1. Numerically Invariant Expressions for  $\kappa$  and  $\kappa_s$ .** Let  $P_{i-1}$ ,  $P_i$  and  $P_{i+1}$  be three consecutive points on a space curve and let  $a$ ,  $b$  and  $c$  be their mutual distances as illustrated in Figure 1. Denote by  $\Delta$  the area of the triangle with sides  $a$ ,  $b$  and  $c$ . The curvature of a space curve is defined exactly the same way as the curvature of a planar curve: it is the inverse of the radius of the osculating circle at  $p$ . So we expect that  $\tilde{\kappa} = \pm \frac{4\Delta}{abc}$  is a good approximation for  $\kappa$  at  $P_i$ . Indeed, a Mathematica routine using the local canonical form of a curve in  $\mathbb{R}^3$  gave us the following Taylor series expansion.

$$\begin{aligned} \tilde{\kappa} &= \kappa + \frac{(b-a)}{3}\kappa_s + (a^2 + b^2)\left(\frac{\kappa_{ss}}{12} - \frac{\kappa\tau^2}{36}\right) - ab\left(\frac{\kappa_{ss}}{12} + \frac{\kappa\tau^2}{36}\right) \\ &+ (b^3 - a^3)\left(\frac{\kappa^2\kappa_s}{40} - \frac{7\kappa_s\tau^2}{570} - \frac{\kappa\tau\tau_s}{45} + \frac{\kappa_{sss}}{60}\right) \\ &+ (a^2b - ab^2)\left(-\frac{\kappa^2\kappa_s}{60} + \frac{\kappa_s\tau^2}{180} + \frac{\kappa\tau\tau_s}{180} + \frac{\kappa_{sss}}{60}\right) + \dots \end{aligned}$$

Note that if we set  $\tau = 0$ , then our result agrees with the 2-dimensional case. Also observe that  $\tau$  does not appear in the first two terms of the expansion. Therefore the expressions for  $\kappa_s$  given in the planar case ((4), (5) and (6)) are valid numerically invariant expressions for  $\kappa_s$  in the three dimensional case.

**3.2. Numerically Invariant Expressions for  $\tau$  and  $\tau_s$ .** The Euclidean invariant torsion  $\tau$  is defined as the derivative of the angle of the osculating plane with respect to arc-length. Let  $-1 \ll -\delta < 0 < \epsilon_1 < \epsilon_2 \ll 1$ . Suppose  $P_{i-1} = \alpha(-\delta)$ ,  $P_i = \alpha(0)$ ,  $P_{i+1} = \alpha(\epsilon_1)$  and  $P_{i+2} = \alpha(\epsilon_2)$  are four consecutive points on a space curve  $\alpha$ . Let  $a$ ,  $b$ ,  $c$ ,  $d$ ,  $e$  and  $f$  be their mutual distances as illustrated in figure 1. Denote by  $H$  the height of the tetrahedron with sides  $a$ ,  $b$ ,  $c$ ,  $d$ ,  $e$  and  $f$  with respect to  $P_{i+2}$  and write  $\Delta_{l_1l_2l_3}$  for the area of a triangle with sides of length  $l_1$ ,  $l_2$  and  $l_3$ .

We propose the two following numerically invariant expressions for the torsion at  $P_i$ :

$$(11) \quad \tilde{\tau}_1 = \pm 6 \cdot \frac{H}{def\tilde{\kappa}}$$

$$(12) \quad \tilde{\tau}_2 = \pm \frac{3}{2} \cdot \frac{Hb}{f\Delta_{abd}}$$

Observe that (11) and (12) both use the minimal number of points (i.e. four since it is a third order derivative) for approximating  $\tau$ . One might argue that this induces an asymmetry in the numerical results. However, that is easy to fix in a practical situation (for example by averaging the results obtained in the two directions).

We justify (11) as follows: It is known that  $\tau = \frac{-\alpha_s \times \alpha_{sss} \cdot \alpha_{sss}}{\kappa^2}$ , [Car76]. In other words,  $|\tau\kappa|$  is the component of  $\alpha_{sss}$  which is perpendicular to the osculating plane. We start by writing down a finite difference scheme for  $\alpha_{sss}$  (for justifications, see [FK93] §5.4).

$$(13) \quad \alpha_{sss}(0) \approx 6 \cdot \frac{\frac{\alpha(\epsilon_2) - \alpha(\epsilon_1)}{\epsilon_2 - \epsilon_1} - \frac{\alpha(\epsilon_1) - \alpha(0)}{\epsilon_1}}{\epsilon_2} - \frac{\frac{\alpha(\epsilon_1) - \alpha(0)}{\epsilon_1} - \frac{\alpha(0) - \alpha(-\delta)}{\delta}}{\delta + \epsilon_1}.$$

As  $\epsilon_1$  and  $\delta$  approach zero, the plane defined by  $P_{i-1}$ ,  $P_i$  and  $P_{i+1}$  approaches the osculating plane. More precisely, if  $\delta$  and  $\epsilon_1$  are small enough, we find (from the local canonical form of the curve) that the equation of the plane passing through  $\alpha(-\delta)$ ,  $\alpha(0)$  and  $\alpha(\epsilon)$  can be written as

$$Ax + By + z = 0$$

with  $A = \frac{\kappa\tau}{6}\epsilon_1\delta + O(3)$  and  $B = -\frac{\tau}{3}(\epsilon_1 - \delta) + O(2)$ . Here,  $x$ ,  $y$  and  $z$  are the Frenet frame coordinates. The normal vector to this plane is  $\frac{(A, B, 1)}{\sqrt{A^2 + B^2 + 1}}$  which is a first order approximation of  $(0, 0, 1)$ , the normal vector to the osculating plane.

We have

$$\begin{aligned}\kappa\tau &= \alpha_{sss} \cdot (0, 0, 1) \\ &= \alpha_{sss} \cdot \frac{(A, B, 1)}{\sqrt{A^2 + B^2 + 1}} + O(1).\end{aligned}$$

But

$$\alpha(-\delta) \cdot (A, B, 1) = \alpha(0) \cdot (A, B, 1) = \alpha(\epsilon_1) \cdot (A, B, 1) = 0$$

and

$$\alpha(\epsilon_2) \cdot \frac{(A, B, 1)}{\sqrt{A^2 + B^2 + 1}} = \pm H.$$

Therefore

$$\begin{aligned}\kappa\tau &\approx \frac{\pm 6H}{(\epsilon_2 - \epsilon_1)\epsilon_2(\delta + \epsilon_2)} \\ &\approx \pm \frac{6H}{def}.\end{aligned}$$

From the previous section we know that  $\kappa \approx \pm \tilde{\kappa} = \frac{4\Delta_{abc}}{abc}$  and therefore  $\tau \approx \pm \frac{6H}{def\tilde{\kappa}}$ .

There is an interesting similarity between (11) and  $\tilde{\kappa}$ . This is easily seen if we write  $\tilde{\kappa}$  in a slightly different way. By a basic geometry argument we can say that  $\tilde{\kappa} = \pm \frac{2h}{ab}$  where  $h$  is the height of the triangle with sides  $a$ ,  $b$  and  $c$ . Thus  $\tilde{\kappa}\tilde{\tau}$  can be looked at as a three dimensional version of  $\tilde{\kappa}$ . This is one reason why we like (11). Another reason is that it provides us with an easy visual understanding of the torsion similar to the understanding we already have of the curvature. It is indeed easier to picture the height and sides of a tetrahedron together with the radius of the osculating circle than a derivative. It makes the evaluation of the torsion from a picture of the curve very intuitive.

To find (12), we started from the following definition: if  $P = \alpha(s)$  and  $Q = \alpha(0)$ , then  $\tau = \lim_{P \rightarrow Q} \frac{\theta}{s}$ , where  $\theta$  is the angle between the osculating planes at  $P$  and  $Q$  respectively [Eve65]. We approximated  $\theta$  by  $\sin \tilde{\theta}$  where  $\tilde{\theta}$  denotes the angle between the plane  $P_i P_{i+1} P_{i+2}$  and the plane  $P_{i-1} P_i P_{i+1}$ . If we assign to the plane  $P_{i-1} P_i P_{i+1}$  the equation  $z = 0$  and if we let the segment  $P_i P_{i+1}$  represent the  $x$ -axis, then the plane passing through  $BCD$  has equation  $Hy - D_y z = 0$  where  $D_y$  is the projection of the point  $D$  on the  $y$ -axis.

Given the equations of two planes  $A_1x + B_1y + C_1z + D_1 = 0$  and  $A_2x + B_2y + C_2z + D_2 = 0$ , the angle between the two planes is given by

$$\cos \theta = \frac{A_1A_2 + B_1B_2 + C_1C_2}{\sqrt{A_1^2 + B_1^2 + C_1^2}\sqrt{A_2^2 + B_2^2 + C_2^2}}.$$

A straightforward computation gives us

$$\begin{aligned} \sin \tilde{\theta} &= \pm \frac{H}{\sqrt{H^2 + D_y^2}} \\ &= \pm \frac{H}{\sqrt{e^2 - D_x^2}} \\ &= \pm \frac{H}{\sqrt{e^2 - \left(\frac{e^2 + b^2 - d^2}{2b}\right)^2}} \\ &= \pm \frac{2Hb}{\sqrt{4e^2b^2 - (e^2 + b^2 - d^2)^2}} \\ &= \pm \frac{2Hb}{4\Delta_{ebd}} \\ &= \pm \frac{Hb}{2\Delta_{ebd}}. \end{aligned} \tag{14}$$

On the other hand, we can use the local canonical form to approximate the equations of the plane  $P_{i-1}P_iP_{i+1}$  and  $P_iP_{i+1}P_{i+2}$  in the Frenet frame coordinates. Respectively, we have approximately

$$\left(\frac{\kappa\tau\epsilon_1\delta}{6}\right)x + \left(\frac{\tau}{3}\right)(\epsilon_1 - \delta)y + z = 0$$

and

$$\left(\frac{-\kappa\tau\epsilon_1\epsilon_2}{6}\right)x + \left(\frac{\tau}{3}\right)(\epsilon_1 + \epsilon_2)y + z = 0.$$

So

$$\cos^2 \tilde{\theta} \approx \frac{\left(1 + \left(\frac{\tau}{3}\right)^2(\epsilon_1 - \delta)(\epsilon_1 + \epsilon_2)\right)^2}{1 + \left(\frac{\tau}{3}(\epsilon_1 - \delta)\right)^2 + \left(\frac{\tau}{3}(\epsilon_1 + \epsilon_2)\right)^2}$$

and therefore

$$\sin^2 \tilde{\theta} \approx \frac{\tau^2}{9}(\epsilon_2 + \delta)^2 \approx \frac{\tau^2}{9}f^2$$

i.e.  $\frac{3\sin \tilde{\theta}}{f} \approx \pm\tau$ . Combining this result with (14), we get (12).

With the help of the symbolic computation software Mathematica and using the local canonical form of a curve, we computed the Taylor series expansion for both expressions. For (11), we obtained

$$(15) \quad \tilde{\tau}_1 = \tau + \frac{\tau \kappa_s}{6\kappa}(a - b + 3e) + \frac{\tau_s}{4}(b - a + e) + O(2).$$

For (12) we obtained

$$(16) \quad \tilde{\tau}_2 = \tau + \frac{\tau \kappa_s}{6\kappa}(a + b + e) + \frac{\tau_s}{4}(b - a + e) + O(2).$$

These expansions prove that (11) and (12) are not equivalent.

There are many ways to approximate  $\tau_s$ . For the reasons mentioned above, we chose to use (11). In a similar way as for  $\kappa_s$ , we used (15) to obtain the following numerically invariant expression for  $\tau_s$ . For symmetry reasons, and in view of the results obtained for  $\kappa_s$ , we decided on using a centered formula. The result is the following five point approximation.

$$(17) \quad \tilde{\tau}_s(P_i) = 4 \cdot \frac{\tilde{\tau}_1(P_{i+1}) - \tilde{\tau}_1(P_{i-1}) + (2a + 2b - 2d - 3h + g) \frac{\tilde{\tau}_1(P_i) \tilde{\kappa}_{s,2}(P_i)}{6\tilde{\kappa}(P_i)}}{2a + 2b + 2d + h + g}$$

Where  $g = d(P_{i-2}, P_{i-1})$  as illustrated on Figure 1 and  $\tilde{\kappa}_s$  can be taken to be either (4), (5) or (6).

**3.3. Numerical Tests.** We considered the curve  $\alpha(t) = (\cos t, \sin t, \sqrt{t})$  whose graph is given in Figure 17. Note that  $\alpha$  is not parameterized by arc length. The signature of this curve is given by the following four quantities:

$$\begin{aligned} \kappa &= |\alpha_{ss}| = \frac{|\alpha_t \times \alpha_{tt}|}{|\alpha_t|^3} = \frac{2\sqrt{16t^3 + 4t^2 + 1}}{(1 + 4t)^{3/2}}, \\ \kappa_s &= \frac{d\kappa}{dt} \frac{dt}{ds} = \frac{\frac{d\kappa}{dt}}{\frac{ds}{dt}} = \frac{8(8t^2 + 2t - 3)\sqrt{t}}{\sqrt{16t^3 + 4t^2 + 1}(1 + 4t)^3}, \\ \tau &= -\frac{\alpha_t \times \alpha_{tt} \cdot \alpha_{ttt}}{|\alpha_t \times \alpha_{tt}|^2} = \frac{-2\sqrt{t}(3 + 4t^2)}{16t^3 + 4t^2 + 1}, \\ \tau_s &= \frac{d\tau}{dt} \frac{dt}{st} = \frac{\frac{d\tau}{dt}}{\frac{ds}{dt}} = \frac{2(64t^5 - 16t^4 + 240t^3 + 16t^2 - 3)}{\sqrt{4t + 1}(16t^3 + 4t^2 + 1)^2}. \end{aligned}$$

We tested our numerical expressions on the portion of the curve given by  $\frac{\pi}{2} \leq t \leq \frac{3\pi}{2}$  for different partition sizes. We used  $\tilde{\kappa}_s$  given by equation (6) for evaluating  $\tilde{\tau}_s$ . Care was taken to partition the curve irregularly. In the example presented in figures 18-22, we computed the signature obtained with a random partition  $\{t_i\}_{i=0}^N$  with maximal step  $\Delta t$  (i.e.  $t_{i+1} - t_i \leq \Delta t, \forall i = 1, \dots, N - 1$ ), for  $\Delta t = 0.1, 0.05, 0.025$  and  $0.0125$ .

For simplicity, we graphed two projections of the signature curve. Although a lot of the information is lost this way, we believe that it gives a good measure of the effectiveness of the method. We can see that although the partition is not regular, the graphs seem to converge to the exact graphs when  $\Delta t$  becomes small. Therefore we believe that our formulas work properly for generic small partitions.

We also wanted to check whether our formulas would work with noisy data. So we added some noise on the spatial curve pictured in Figure 17 to see what would be the effect on our signature. This was done by replacing  $(\cos t_i, \sin t_i, \sqrt{t_i})$  by  $(\cos t_i + r_{i,1}\epsilon, \sin t_i + r_{i,2}\epsilon, \sqrt{t_i} + r_{i,3}\epsilon)$  with  $0 \leq r_{i,1}, r_{i,2}, r_{i,3} \leq 1$  three random numbers. Some of the results obtained with  $\epsilon = 0.1$  are shown in Figures 23 and 24. According to the graph, our approximations also seem to be valid even with noisy data points.

#### 4. CONCLUSION

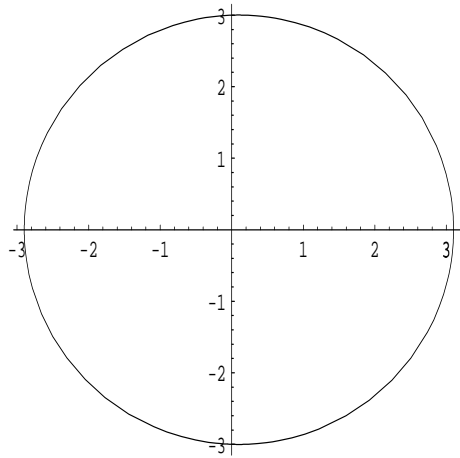
We now have in our hands good approximations for the Euclidean and affine signature of a planar curve. The formulas we obtained are invariant under the action of the Euclidean and affine group respectively. Another important property is that they are valid for any fine partition of the given curve. In the near future, we hope to use them for the recognition of planar curves and perhaps also for some other applications as well. In particular, we wish to prove that the signature can be a practical tool for object recognition, at least in the planar Euclidean case.

We also have good approximations for the four differential invariants which parameterize the Euclidean signature of a space curve, namely the curvature, the torsion and their derivatives with respect to arc length. The formulas we obtained are Euclidean invariants and valid for any fine partition of the given curve. In particular, we showed in section 3 that  $\tilde{\tau} = \pm 6 \cdot \frac{H}{def\kappa}$  is a good approximation for the torsion. We believe that this expression has a value on its own as it gives an easy visual understanding of the concept of torsion. Space curve recognition (for example blood vessels or trajectory of particles) is an interesting computer vision problem where our formulas could find applications.

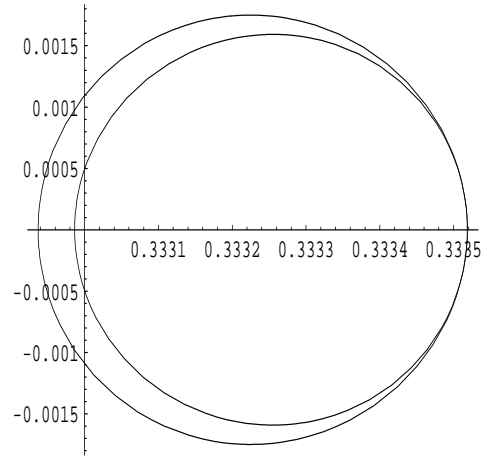
## ACKNOWLEDGMENTS

I want to thank my advisor Peter J. Olver for his advice and support. I would also like to thank Allen Tannenbaum for stimulating discussions and Steve Haker for letting me use code of his for the affine signature and the segmentation/denoising of the pictures as well as for buying and taking pictures of the hardware used for this paper.

FIGURE 2. Exact Data Used for Testing the Planar Euclidean Case.



The Curve  $r = 1 + \frac{1}{10} \cos t$



Corresponding Euclidean signature.

FIGURE 3. Three Different Partitions of the Initial Curve Used in the Planar Euclidean Case.

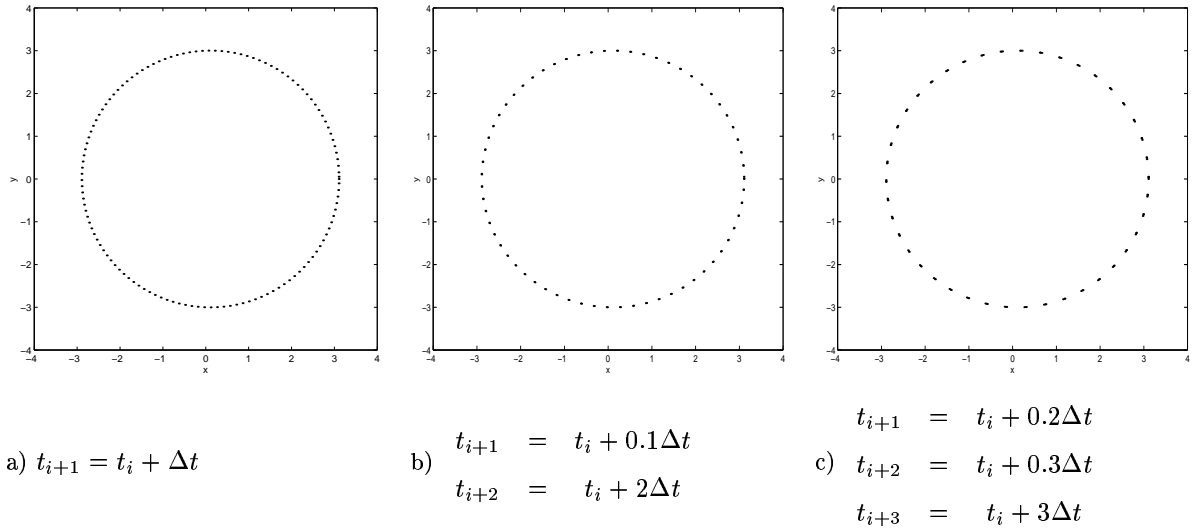


FIGURE 4. Approximations of the Euclidean Signature Curve Obtained with (2).

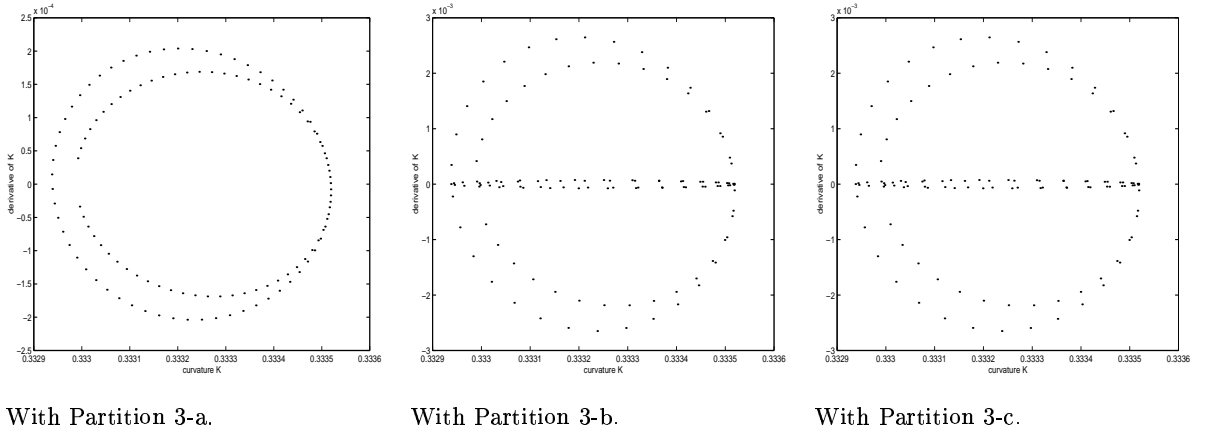
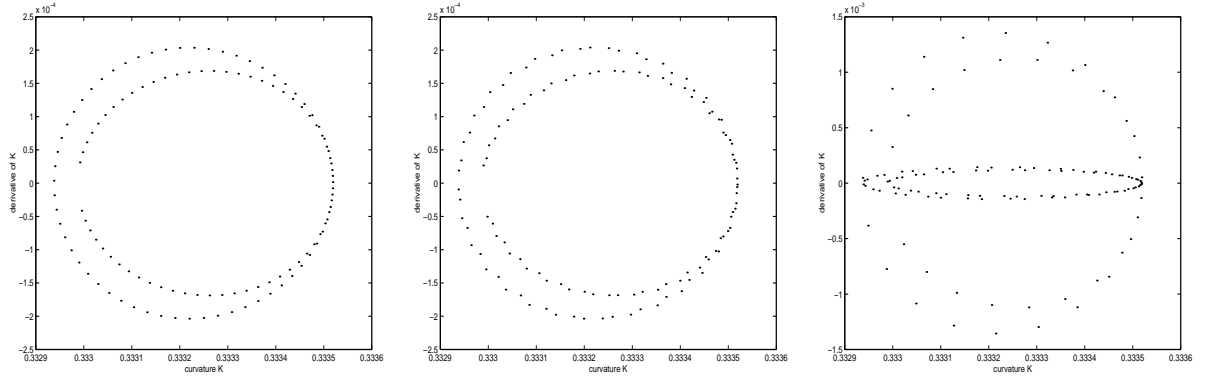


FIGURE 5. Approximations of the Euclidean Signature Curve Obtained with (3).

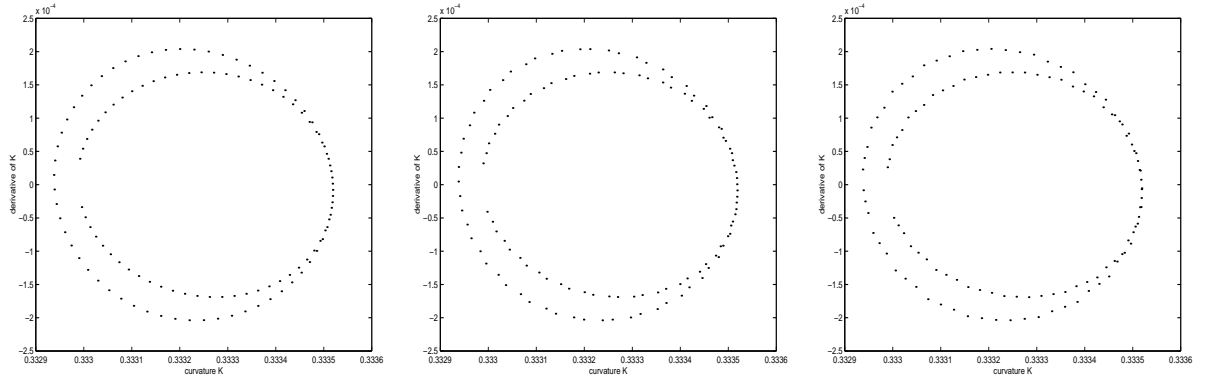


With Partition 3-a.

With Partition 3-b.

With Partition 3-c.

FIGURE 6. Approximations of the Euclidean Signature Curve Obtained with (4).

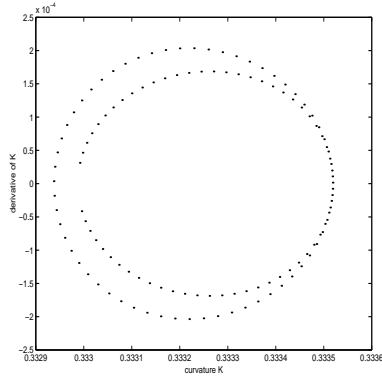


With Partition 3-a.

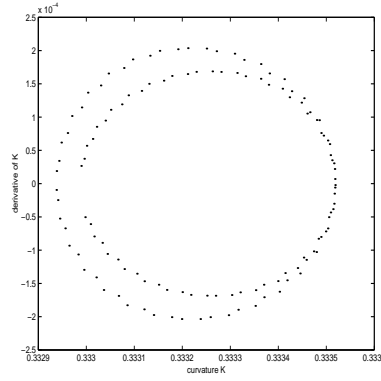
With Partition 3-b.

With Partition 3-c.

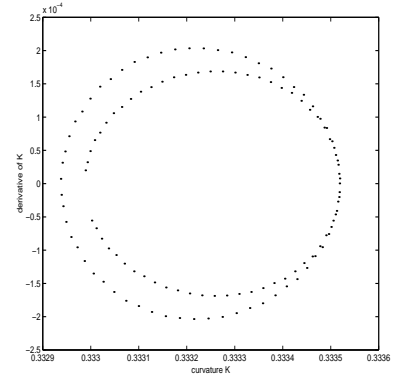
FIGURE 7. Approximations of the Euclidean Signature Curve Obtained with (5).



With Partition 3-a.

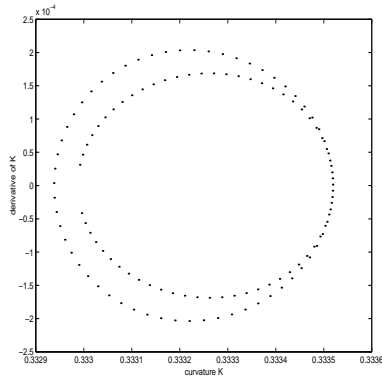


With Partition 3-b.

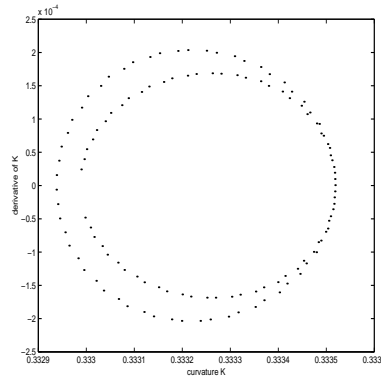


With Partition 3-c.

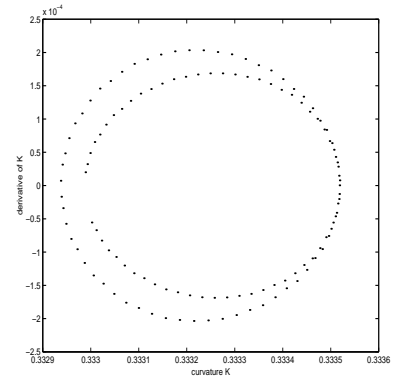
FIGURE 8. Approximation of the Euclidean Signature Curve Obtained with (6).



With Partition 3-a.

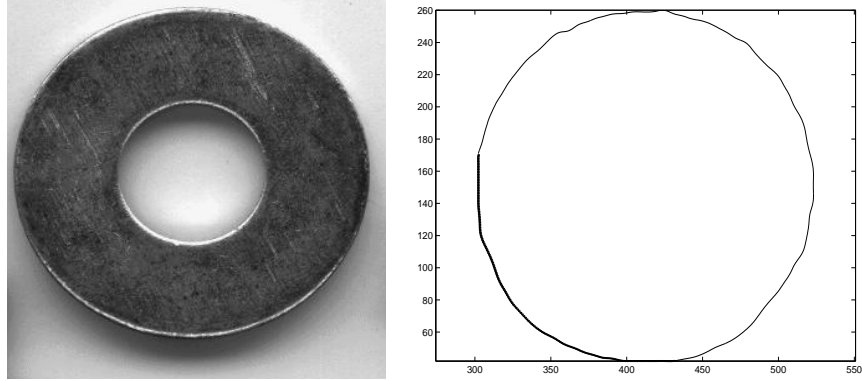


With Partition 3-b.



With Partition 3-c.

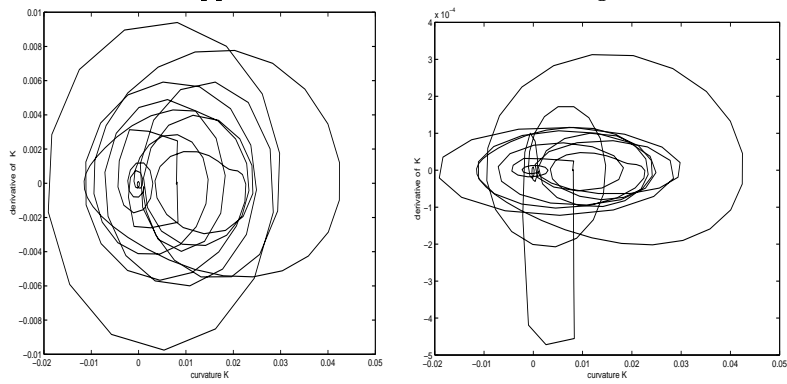
FIGURE 9. Noisy Data Used for Testing the Planar Euclidean Case.



Picture of a washer.

Segmented boudary.

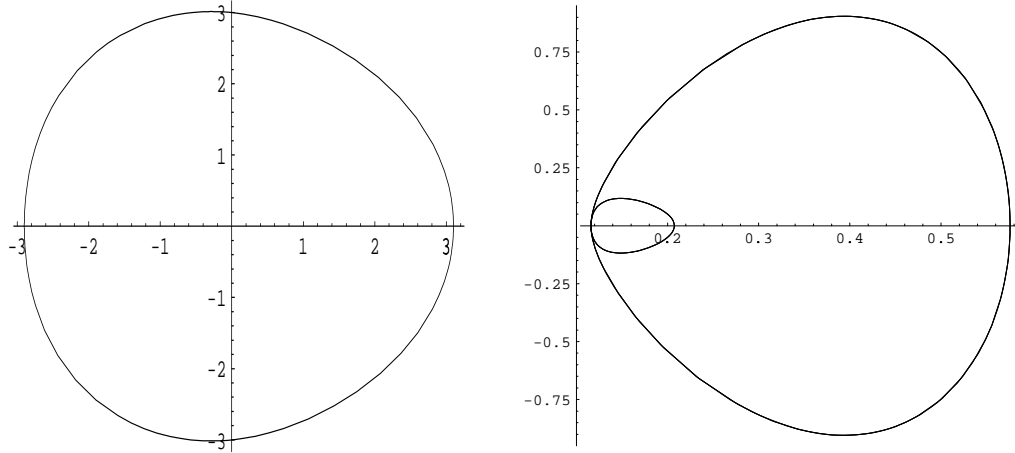
FIGURE 10. Approximations of the Euclidean Signature Curve.



Signature obtained with (3)

Signature obtained with (6)

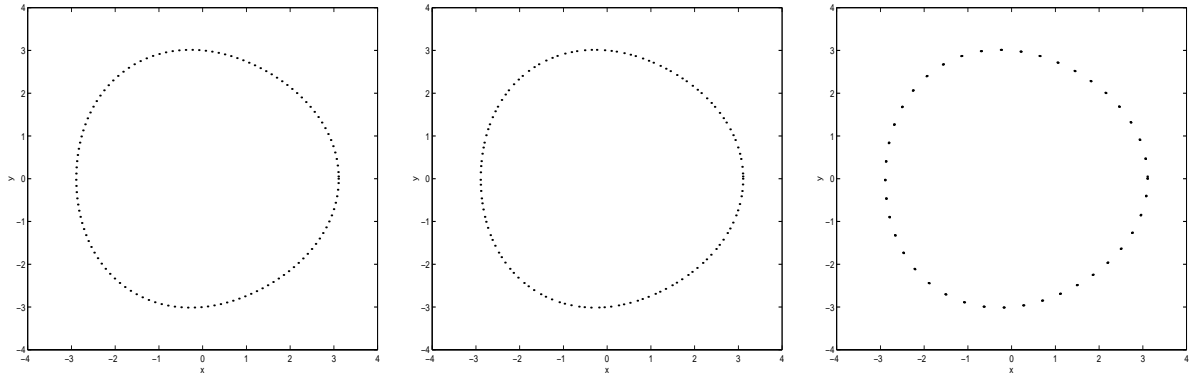
FIGURE 11. Exact Data Used for Testing the Planar Affine Case.



The Curve  $r = 1 + \frac{1}{10} \cos 3t$

Corresponding affine signature.

FIGURE 12. Three Different Partitions of the Initial Curve Used in the Planar Affine Case.



a)  $t_{i+1} = t_i + \Delta t$

$$t_{i+1} = t_i + 0.8\Delta t$$

$$b) \quad t_{i+2} = t_i + 1.8\Delta t$$

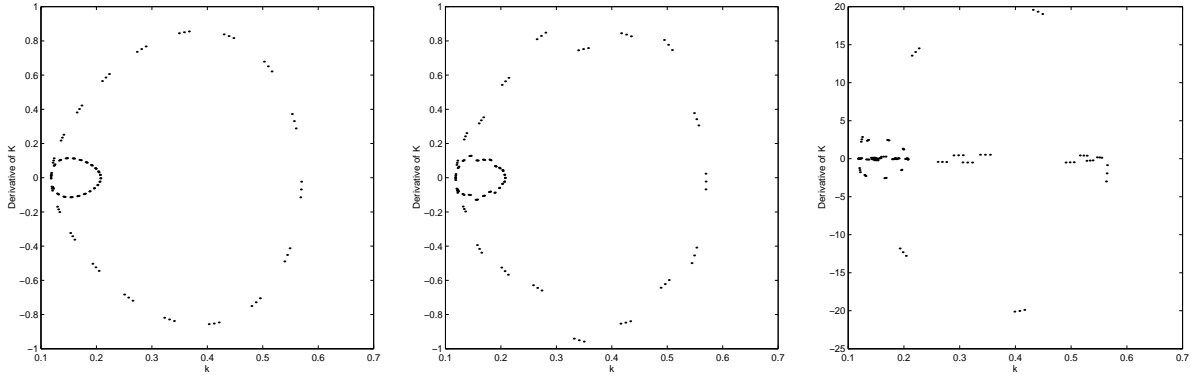
$$t_{i+3} = t_i + 3\Delta t$$

$$t_{i+1} = t_i + 0.01\Delta t$$

$$c) \quad t_{i+2} = t_i + 0.1\Delta t$$

$$t_{i+3} = t_i + 3\Delta t$$

FIGURE 13. Approximations of the Affine Signature Curve Obtained with (9).

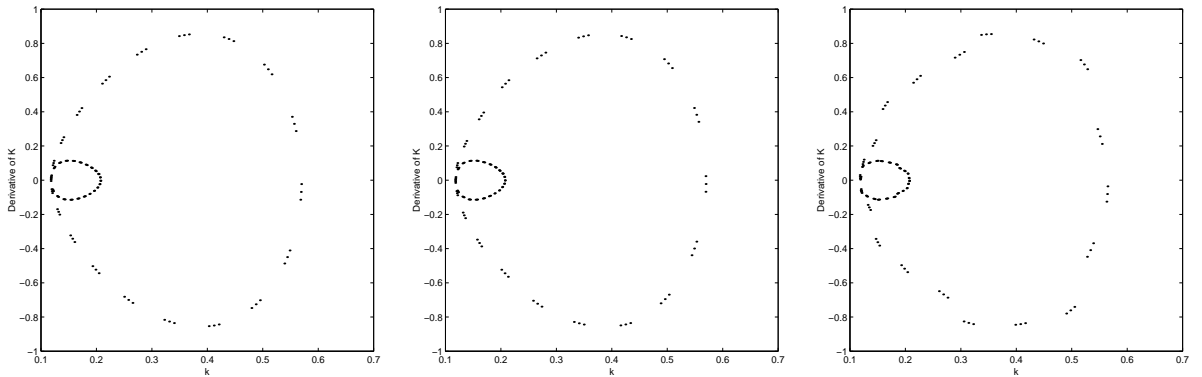


With partition 10-a.

With partition 10-b.

With partition 10-c.

FIGURE 14. Approximations of the Affine Signature Curve Obtained with (10).



With Partition 10-a.

With Partition 10-b.

With Partition 10-c.

FIGURE 15. Noisy Data Used for Testing the Planar Affine Case.

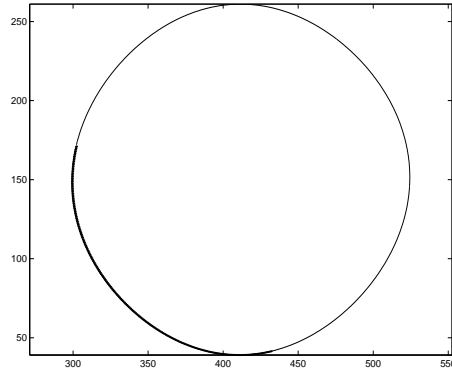
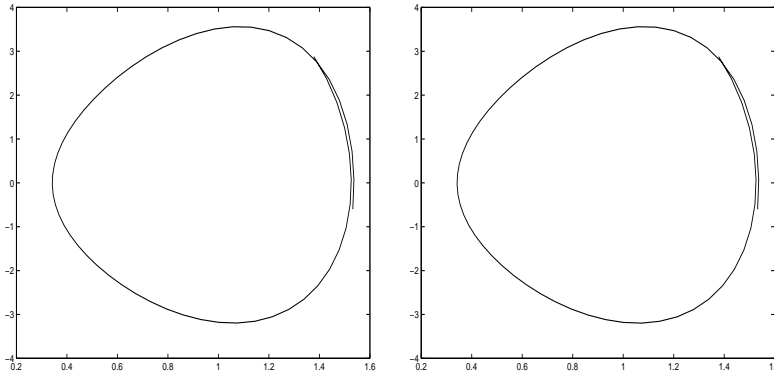


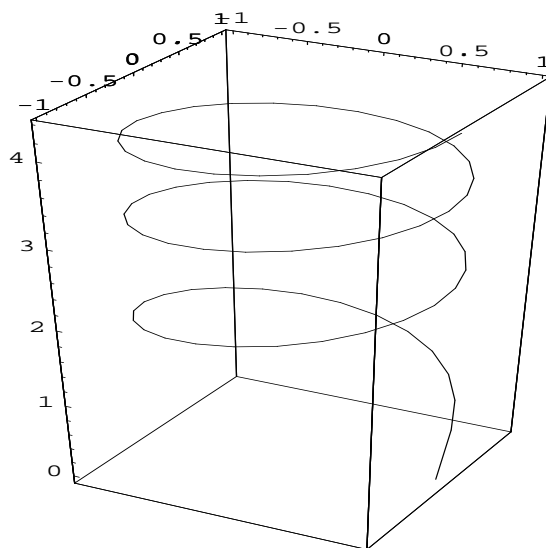
FIGURE 16. Approximations of the Affine Signature Curve.



Signature obtained with (9)

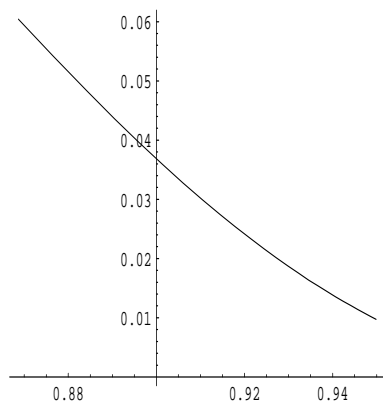
Signature obtained with (10)

FIGURE 17. Curve Used to Test the Formulas Proposed for the Spatial Signature

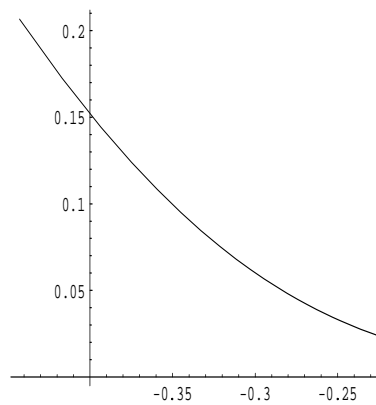


The Curve  $\alpha(t) = (\cos t, \sin t, \sqrt{t})$ , for  $0 \leq t \leq 6\pi$

FIGURE 18. Projections of the Exact Signature for our Test Curve



Derivative of the Curvature vs Curvature



Derivative of the Torsion vs Torsion

FIGURE 19. Approximations of  $(\kappa, \kappa_s)$  Obtained with 67 Random Points ( $\Delta t \leq 0.1$ )

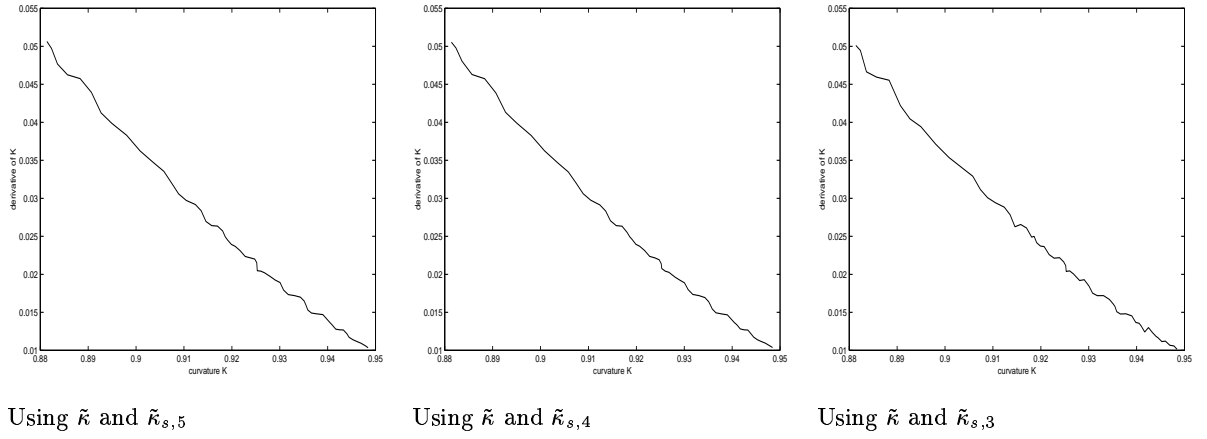


FIGURE 20. Approximations of  $(\kappa, \kappa_s)$  Obtained with 248 Random Points ( $\Delta t \leq 0.025$ )

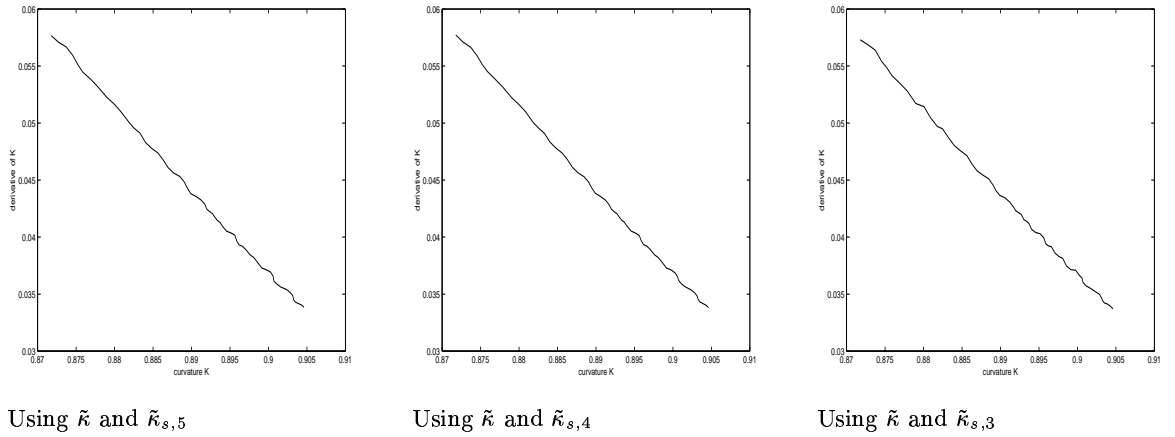
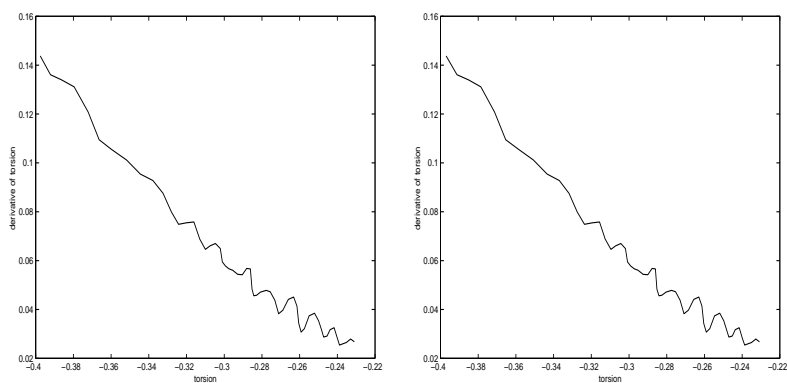


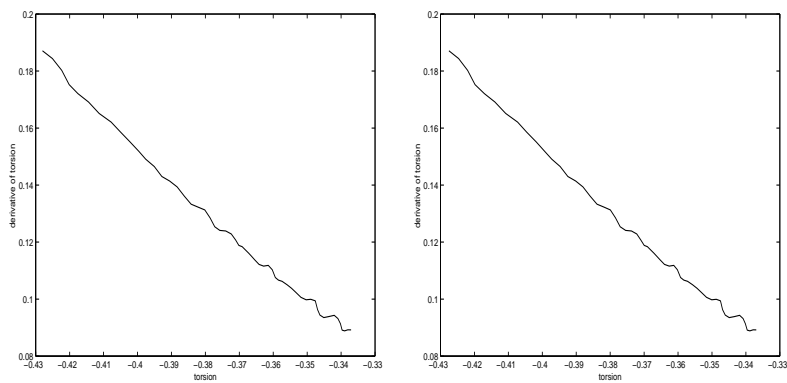
FIGURE 21. Approximations of  $(\tau, \tau_s)$  Obtained with 67 Random Points ( $\Delta t \leq 0.1$ )



Using  $\tilde{\tau}_1$  and  $\tilde{\tau}_s$

Using  $\tilde{\tau}_2$  and  $\tilde{\tau}_s$

FIGURE 22. Approximations of  $(\tau, \tau_s)$  Obtained with 248 Random Points ( $\Delta t \leq 0.025$ )



Using  $\tilde{\tau}_1$  and  $\tilde{\tau}_s$

Using  $\tilde{\tau}_2$  and  $\tilde{\tau}_s$

FIGURE 23. Approximations of  $(\kappa, \kappa_s)$  Obtained with 130 Random and Noisy Data Points ( $\Delta t \leq 0.025$ ,  $\epsilon = 0.1$ )

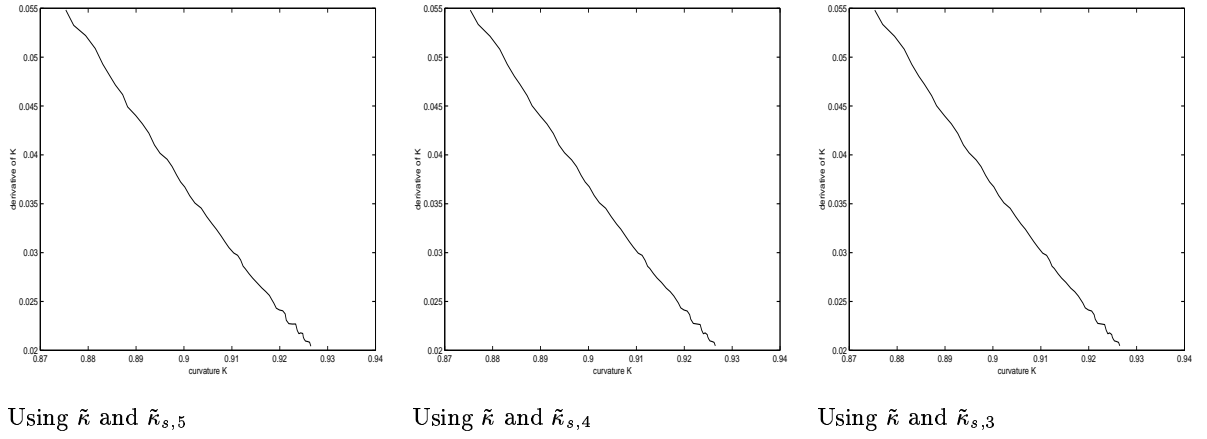
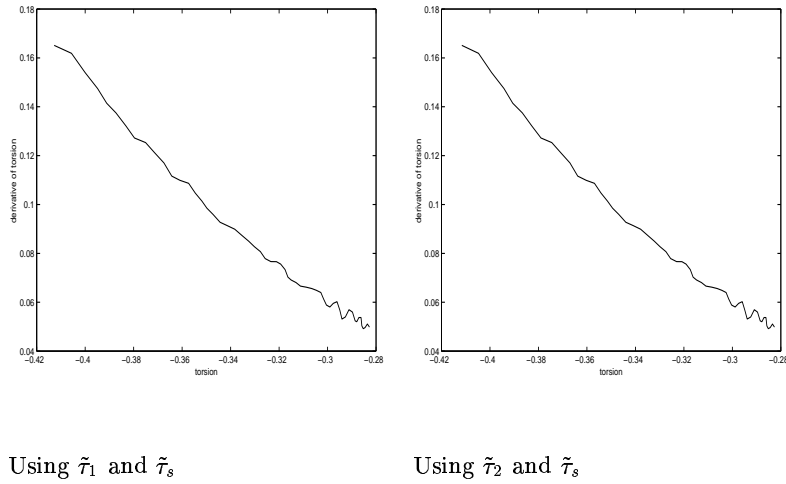


FIGURE 24. Approximations of  $(\tau, \tau_s)$  Obtained with 130 Random and Noisy Data Points ( $\Delta t \leq 0.025$ ,  $\epsilon = 0.1$ )



## REFERENCES

- [Car35] É. Cartan. *La méthode du repère mobile, la théorie des groupes continus et les espaces généralisés*. Exposés de géométrie No.5. Hermann, Paris, 1935.
- [Car76] M. P. Do Carmo. *Differential Geometry of Curves and Surfaces*. Prentice-Hall, 1976.
- [COS<sup>+</sup>98] E. Calabi, P. J. Olver, C. Shakiban, A. Tannenbaum, and S. Haker. Differential and numerically invariant signature curves applied to object recognition. *Int. J. Comput. Vision*, 26:107–135, 1998.
- [Eve65] H. Eves. *A Survey of Geometry, II*. Allyn and Bacon, 1965.
- [FK93] M. Friedman and A. Kandel. *Fundamentals of Computer Numerical Analysis*. CRC, Boca Raton, 1993.

## LIST OF FIGURES

1	Definition of Variables Used for Distances	3
2	Exact Data Used for Testing the Planar Euclidean Case.	15
3	Three Different Partitions of the Initial Curve Used in the Planar Euclidean Case.	16
4	Approximations of the Euclidean Signature Curve Obtained with (2).	16
5	Approximations of the Euclidean Signature Curve Obtained with (3).	17
6	Approximations of the Euclidean Signature Curve Obtained with (4).	17
7	Approximations of the Euclidean Signature Curve Obtained with (5).	18
8	Approximation of the Euclidean Signature Curve Obtained with (6).	18
9	Noisy Data Used for Testing the Planar Euclidean Case.	19
10	Approximations of the Euclidean Signature Curve.	19
11	Exact Data Used for Testing the Planar Affine Case.	20
12	Three Different Partitions of the Initial Curve Used in the Planar Affine Case.	20
13	Approximations of the Affine Signature Curve Obtained with (9).	21
14	Approximations of the Affine Signature Curve Obtained with (10).	21
15	Noisy Data Used for Testing the Planar Affine Case.	22
16	Approximations of the Affine Signature Curve.	22
17	Curve Used to Test the Formulas Proposed for the Spatial Signature	23
18	Projections of the Exact Signature for our Test Curve	23
19	Approximations of $(\kappa, \kappa_s)$ Obtained with 67 Random Points ( $\Delta t \leq 0.1$ )	24
20	Approximations of $(\kappa, \kappa_s)$ Obtained with 248 Random Points ( $\Delta t \leq 0.025$ )	24
21	Approximations of $(\tau, \tau_s)$ Obtained with 67 Random Points ( $\Delta t \leq 0.1$ )	25
22	Approximations of $(\tau, \tau_s)$ Obtained with 248 Random Points ( $\Delta t \leq 0.025$ )	25
23	Approximations of $(\kappa, \kappa_s)$ Obtained with 130 Random and Noisy Data Points ( $\Delta t \leq 0.025, \epsilon = 0.1$ )	26

24	Approximations of $(\tau, \tau_s)$ Obtained with 130 Random and Noisy Data Points ( $\Delta t \leq 0.025$ , $\epsilon = 0.1$ )	26
----	--	----